J. Fluid Mech. (2006), *vol.* 554, *pp.* 5–24.
doi:10.1017/S0022112005008104 Printed in the United Kingdom

The spreading and stability of a surfactant-laden drop on a prewetted substrate

By O. E. JENSEN[1] AND S. NAIRE[2]

[1]School of Mathematical Sciences, University of Nottingham, University Park, Nottingham NG7 2RD, UK

[2]Department of Mathematics, Heriot-Watt University, Riccarton, Edinburgh EH14 4AS, UK

(Received 17 February 2005 and in revised form 23 August 2005)

We consider a viscous drop, loaded with an insoluble surfactant, spreading over a flat plane that is covered initially with a thin liquid film. Lubrication theory allows the flow to be modelled using coupled nonlinear evolution equations for the film thickness and surfactant concentration. Exploiting high-resolution numerical simulations, we describe the multi-region asymptotic structure of the spatially one-dimensional spreading flow and derive a simplified ODE model that captures its dominant features at large times. The model includes a version of Tanner's law accounting for a Marangoni flux through the drop's effective contact line, the magnitude of which is influenced by a rarefaction wave in the film ahead of the contact line. Focusing on the neighbourhood of the contact line, we then examine the stability of small-amplitude disturbances with spanwise variation, using long-wavelength asymptotics and numerical simulations to describe the growth-rate/wavenumber relationship. In addition to revealing physical mechanisms and new scaling properties, our analysis shows how initial conditions and transient dynamics have a long-lived influence on late-time flow structures, spreading rates and contact-line stability.

1. Introduction

Surfactants are chemicals that adsorb at interfaces to change the local surface tension. They are exploited in many areas of technology to control the wetting properties of liquids on solid surfaces. Common applications include detergency, crop-spraying, coating processes, microfluidics and oil recovery. Whether their presence is desired or not, surface-active materials pervade most areas of interfacial fluid mechanics. Their importance is reflected by a significant increase since the early 1990s in the number of papers in the *Journal of Fluid Mechanics* concerned with surfactant-mediated flows. The mammalian lung has motivated much recent research in this area (Grotberg 1994, 2001; Gaver, Halpern & Jensen 2005). Natural lung surfactant, a complex mixture of phospholipids and proteins, performs many important physiological roles including maintenance of the mechanical stability and compliance of liquid-lined airways and alveoli. Its fundamental biomechanical significance is illustrated by evidence that the development of lung surfactant was a prerequisite for evolution of the vertebrate lung and of air-breathing (Daniels 2001). In modern times, surfactant replacement therapy has become a standard life-saving treatment for premature infants who are born with an immature surfactant system. Motivated in part by this application, we address here a long-standing and challenging

problem in thin-film fluid mechanics: the spreading and stability of a surfactant-laden drop on a surface coated with an initially uniform (and surfactant-free) liquid film.

To set this problem in context, it is useful first to recall some key features of drop spreading under spatially uniform surface tension. This is a problem that has attracted enormous attention because of the difficulty of modelling a moving contact line, namely that imposing the no-slip condition at a moving solid/liquid/vapour contact line leads to a non-integrable stress singularity. Numerous regularizations of this singularity have been proposed: a small amount of slip or a precursor film are commonly introduced in order to yield a well-posed problem (e.g. Oron, Davis & Bankoff 1997). The relationship between the speed of the contact line (expressed as a capillary number Ca) and the drop's dynamic contact angle, often called 'Tanner's law' (also credited to Hoffman and Voinov), then includes a logarithmic dependence on the ratio of some inner lengthscale (a slip length, or a precursor film thickness) to the drop radius. While Tanner's law is therefore only weakly dependent on the regularization used, the presence of a logarithm also indicates that there is not the strong separation of lengthscales that facilitates an accurate asymptotic approximation (King 2001). While the contact line of a drop spreading under the effects of surface tension alone is generally stable, when spreading is externally forced (for example by gravity, centrifugal forces, or shear stresses), a bulge is created behind the contact line that can become unstable to a fingering instability with a well-defined wavelength (e.g. Bertozzi & Brenner 1997).

In the presence of surfactant, the macroscopic behaviour of a spreading drop becomes much more sensitive to the delicate physical processes operating near the contact line. Here it helps to distinguish between cases in which there is a precursor film ahead of the drop (such as an aqueous film that adsorbs on a hydrophilic substrate in a humid environment) and those in which the surface ahead of the drop is dry (e.g. a hydrophobic substrate in a low-humidity environment) (Frank & Garoff 1995). In the former case (exemplified by a surfactant that is electrostatically repelled from the solid substrate), spreading is often accompanied by a dramatic dendritic fingering instability (illustrated in figure 1), the origins of which we consider below; this instability is of a character quite distinct from the spatially regular fingering of a driven contact line mentioned above. In the latter case (exemplified by a surfactant that adsorbs strongly onto the substrate), spreading can have a stick–slip character; for example, the surfactant may diffuse ahead of the drop and adsorb onto the solid/vapour interface (e.g. Starov, Kosvintsev & Velarde 2000) giving rise to 'autophobing' behaviour (in which the surfactant drop will not advance over its own monolayer), resulting in transient drop retraction.

For drops spreading in the absence of a precursor film, the rolling motion of the flow near an advancing contact line causes surfactant at the liquid/vapour interface to accumulate at the contact line (assuming the affinity of the surfactant for the solid is not too high). Marangoni flows (driven by gradients of surface tension) can then immobilize the interface locally. While spreading on hydrophobic substrates is therefore generally slow, 'superspreading' surfactants (the best known examples of which are trisiloxane surfactants) can spread relatively rapidly over hydrophobic substrates by exploiting Marangoni flow. Two important factors are implicated in generating this flow: the presence of surfactant aggregates in the bulk (e.g. a dispersed phase of vesicles; Stoebe *et al.* 1997) and the presence of a precursor film in a humid atmosphere (Zhu *et al.* 1994). Churaev *et al.* (2001) have shown how these two effects may interact, with repulsion between vesicles providing an effective disjoining pressure that prevents severe thinning of the precursor film immediately ahead of the drop

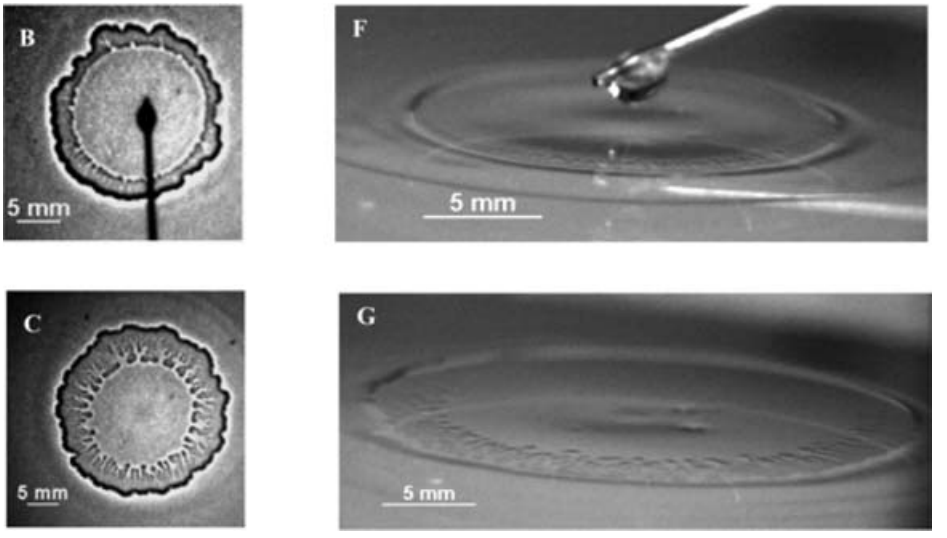

FIGURE 1. Experimental images of surfactant spreading in plan (left) and side (right) views, at early (top) and later (bottom) times. The fingers at the edge of the bulk drop are spreading over an ultra-thin film; this film thickens abruptly across the dark (and slightly irregular) rim (left). Reprinted with permission from Afsar-Siddiqui, Luckham & Matar (2003*b*). Copyright (2003) American Chemical Society.

that would otherwise hinder spreading. The origins of superspreading remain an area of active debate.

In contrast to the extensive literature on the spreading of uncontaminated drops on non-wetting surfaces, relatively few authors have examined the effects of a surfactant in such situations theoretically. Assuming that the surfactant is insoluble and its transport is convection-dominated, Cox (1986) determined the quasi-steady flow in a wedge-shaped region intermediate between the 'outer' bulk drop and the 'inner' zone at the contact line where microscopic physical mechanisms (such as slip) are required to regularize the stress singularity. Since slip reduces to zero the speed of the interface at the contact line (Ramé 2001), Cox (1986) therefore had to assume zero surfactant transfer through the contact line, requiring the interface to be immobile. He derived a modification of Tanner's law valid in the limit $Ca\log(\varepsilon) = O(1)$, where $\varepsilon \ll 1$ is the ratio of the slip length to the drop radius. The modified law is applicable to a large range of contact angles and shows a variety of exotic properties, including non-existence of solutions for certain parameter values, with interesting consequences for contact-line stability. Similarly, Chesters & Elyousfi (1998) showed that surfactant increases the dynamic contact angle for a given Ca and permits multiple solutions. In contrast, Joanny (1989) allowed for transport through the contact line (either allowing surfactant to adsorb onto the solid surface or to escape into a precursor film) and derived a version of Tanner's law including a parameterized Marangoni term, valid for small contact angles.

Ramé (2001) extended Cox's quasi-steady analysis to allow for surfactant transport through the contact line, showing how diffusion into the bulk in the 'inner' region (when slip is present) may provide such a flux. Allowing for Marangoni flow along the drop interface in Cox's 'intermediate' region, assuming a large static contact angle and a fixed surfactant flux through the contact line, Ramé showed how the relationships between dynamic contact angle and contact line speed can be multivalued (providing

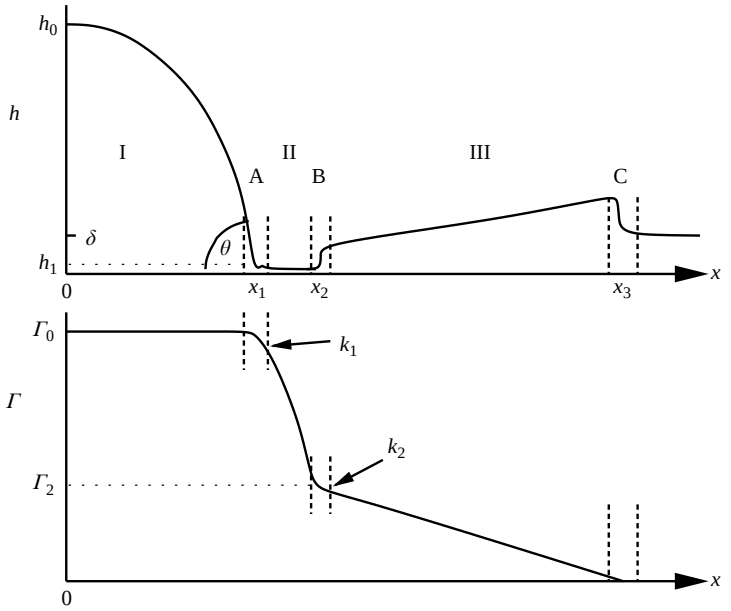

FIGURE 2. A sketch of a droplet spreading on a thin film, showing film thickness h and surfactant concentration Γ as functions of distance x from the drop centre. Dashed lines demarcate asymptotic regions: the bulk drop (I), the ultra-thin film (II), the spreading monolayer (III), the drop's effective contact line (A), the rarefaction wave (B) and the kinematic shock (C).

a possible mechanism for contact-angle hysteresis) and undefined at large speeds. An alternative approach was taken by Clay & Miksis (2004), who examined drop spreading using a specified relation between contact angle and contact-line speed, prescribing the rate of surfactant transfer through the contact line and the dependence of equilibrium contact angle on surfactant concentration; using a model based on lubrication theory, they showed how surfactant slows spreading by interfacial immobilization unless transfer through the contact line is significant. Likewise, Chan & Borhan (2005) (using a similar class of model but employing a nonlinear surface equation of state) showed how droplet spreading rates can be increased by surfactant under suitable conditions.

Surfactant transport through the contact line is an inescapable feature of surfactant-laden drops spreading on a precursor film. Numerous authors have shown experimentally how such spreading gives rise to a dendritic fingering instability at the edge of the drop (e.g. Marmur & Lelah 1981; Troian, Wu & Safran 1989; Zhu *et al.* 1994; He & Ketterson 1995; Cachile *et al.* 2002; Afsar-Siddiqui, Luckham & Matar 2003*a*, *b*; see figure 1); for a detailed review see Asfar-Siddiqui *et al.* (2003*c*). The following sequence of events is believed to give rise to this behaviour. After initial deposition of the drop, a large surface-tension difference exists between the edge of the drop and the precursor film. This is relieved by viscous dissipation in a Marangoni flow of the precursor film, in which a surfactant monolayer (possibly accompanied by surfactant dissolved in the liquid) spreads rapidly over the film. Strong stretching of the film's interface causes film thickening at the leading edge of the monolayer and thinning at the monolayer's upstream end, just ahead of the drop's contact line (an example is sketched in figure 2). The drop therefore has to spread over an

extremely thin, surfactant-loaded liquid layer. In doing so the advancing contact line can develop striking fingering patterns.

Theoretical models of this instability have been developed within the framework of lubrication theory. Troian, Herbolzheimer & Safran (1990) described some of the key features of the overall flow, including a kinematic shock at the leading edge of the insoluble monolayer (previously identified by Borgas & Grotberg 1988), and they proposed a physical mechanism giving rise to fingering in qualitative terms. Roughly speaking, a forward perturbation of the contact line compresses the monolayer in the ultra-thin film immediately ahead of the drop, increasing the surfactant gradient locally; the enhanced Marangoni flow pulls the contact line forward, amplifying the disturbance. Because the drop behind the contact line is relatively deep, perturbations in surfactant concentration equilibrate quickly, suppressing effects that might restrain the growth of the instability. Identifying an 'adverse mobility gradient' (in film depth), Troian *et al.* (1990) suggested an analogy with viscous fingering in a Hele-Shaw cell (or in porous media) in which a more mobile (less viscous) fluid displaces a less mobile one (Homsy 1987). However they were unable to demonstrate this analogy rigorously.

Following this study there was a sustained effort to provide a more quantitative description of the instability. Jensen & Grotberg (1992) showed how an insoluble surfactant monolayer spreading on an initially planar film can be described using a variety of similarity solutions (see also Jensen 1994), so that in a planar geometry a localized monolayer increases in length like $t^{1/3}$ at time t. This algebraically simple solution was an attractive starting point for further analysis. A series of studies examining the stability of this solution to time-dependent perturbations with spanwise variation (Matar & Troian 1997, 1998, 1999*a*; Fischer & Troian 2003*a*) showed that disturbances may exhibit transient algebraic growth, but none showed sustained exponential growth. Sustained growth was however recently reported for disturbances to a $t^{1/2}$ similarity solution associated with continual supply from a source of surfactant (Fischer & Troian 2003*b*), for which severe film thinning near the source leads to a bottleneck in surfactant transport, although the connection between the $t^{1/2}$ similarity solution and drop spreading was not established. A sustained instability was also generated by introducing van der Waals effects, so that film rupture acts as a secondary instability following primary thinning of the film (Matar & Troian 1999*b*). However since fingering is promoted by spreading on hydrophilic rather than hydrophobic surfaces, and by surfactants that are repelled rather than attracted to the interface (Frank & Garoff 1995), the physical origins of this instability are not consistent with those giving rise to dendritic fingering.

More recently, Warner, Craster & Matar (2004*a*) examined the stability of a bulk surfactant-laden drop, from which a monolayer spreads over a thin precursor film, describing the flow using two coupled nonlinear evolution equations for the film thickness and insoluble surfactant concentration (see (2.1) below). In the absence of perturbations, their spatially one-dimensional simulations revealed a structure broadly similar to that described by Troian *et al.* (1990), with severe film thinning immediately ahead of the bulk drop (as illustrated in figure 1). This constriction inhibits the flux of surfactant out of the drop to such an extent that the $t^{1/3}$ (rather than the $t^{1/2}$) similarity solution describes the monolayer flow ahead of the drop. Two types of linear stability analysis of this spatially non-uniform and time-dependent basic state were then undertaken, one examining the growth of perturbations measured by a suitable norm, the other examining the growth of perturbations to a 'frozen' basic state. Both convincingly revealed sustained growth of disturbances concentrated around the edge

of the drop. Computations of the fully nonlinear problem, which are challenging because of the diverse lengthscales that arise, then revealed fingering patterns that resemble those seen experimentally.

In this paper, we revisit the spatially one-dimensional spreading of a surfactant-laden drop treated by Warner *et al.* (2004*a*), using asymptotic approximations to obtain a second-order ODE model for the coupled spreading of the drop and monolayer. This includes a modification of Tanner's law which links the dynamics of the drop's advancing contact line to the Marangoni flow in the ultra-thin film ahead of it. In contrast to previous studies where surfactant transport appears as a prescribed parameter (e.g. Joanny 1989; Ramé 2001; Clay & Miksis 2004), here this flux is determined dynamically. We also identify a new shock structure that may arise (a rarefaction wave) connecting the ultra-thin film to the spreading monolayer, and we highlight the long-lived local influence of the initial conditions. We then examine the stability of the advancing contact line of the drop. Assuming it advances slowly enough that we may treat the base state (described by the familiar Landau–Levich equation) as quasi-steady, a linear stability analysis reveals exponential growth rates for disturbances as a function of spanwise wavenumber. We describe this relationship in the limit of small wavenumber asymptotically and finite-wavenumber effects numerically. This enables us to clarify the proposed analogy with Hele-Shaw fingering and to identify new scaling properties of the instability.

2. The model

We consider the spreading of a drop of surfactant-laden liquid on a flat plane that is prewetted with a thin layer of the same liquid, uncontaminated by surfactant. Initially the drop has maximum height $H^\star$ and width $H^\star/\epsilon$ (for some $\epsilon \ll 1$); the precursor layer has thickness $\delta H^\star$ (for some $\delta \ll 1$) and uniform surface tension $\sigma^\star$. The liquid has constant viscosity $\mu^\star$ and the spreading motion is assumed slow enough that inertial effects may be neglected. Insoluble surfactant is present on the drop initially at concentration $\Gamma^\star$, lowering the surface tension of the drop to $\sigma^\star - S^\star$ ($S^\star$ being the drop's spreading coefficient). The surfactant is assumed sufficiently dilute that $S^\star \ll \sigma^\star$, so that the equation of state relating surface tension to surfactant concentration may be assumed linear (with slope $-S^\star/\Gamma^\star$). The surfactant diffuses on the interface with diffusivity $D^\star$ (a weak effect included here only to regularize numerical solutions). To keep the model as simple as possible we neglect numerous effects that may be significant in experiment (electrostatic forces, gravity, evaporation, van der Waals forces, surface viscosity, etc.). For a detailed survey of such effects in this context see Afsar-Siddiqui *et al.* (2003*c*).

Lubrication theory can be used to derive evolution equations governing the spreading of the drop over the film (Gaver & Grotberg 1990; Jensen & Grotberg 1992; Warner *et al.* 2004*a*). Scaling the film height on $H^\star$, distance along the plane on $H^\star/\epsilon$, time on $\mu^\star H^\star/\epsilon^2 S^\star$, and surfactant concentration on $\Gamma^\star$, the equations are

$$h_t = \nabla\cdot\left(\tfrac{1}{2}h^2\nabla\Gamma + \tfrac{1}{3}h^3\nabla p\right), \quad p = -C\nabla^2 h, \tag{2.1a}$$

$$\Gamma_t = \nabla\cdot\left(h\Gamma\nabla\Gamma + \tfrac{1}{2}h^2\Gamma\nabla p\right) + D\nabla^2\Gamma, \tag{2.1b}$$

where $h(x, y, t)$ is the film thickness, $p(x, y, t)$ the film pressure and $\Gamma(x, y, t)$ the surfactant concentration. Transport is driven by surface tension gradients (represented by terms proportional to $\nabla\Gamma$), capillary pressure gradients and surface diffusion. We work in the domain $x \geqslant 0$, $0 \leqslant y \leqslant 2\pi/k$ for some fixed k, and

impose the boundary conditions $h_x = h_{xxx} = 0$ and $\Gamma_x = 0$ at $x = 0$, $h \to \delta$ and $\Gamma \to 0$ as $x \to \infty$ and periodicity in y. Following Warner *et al.* (2004*a*), the initial conditions are $h(x, y, 0) = \delta + (1-\delta-x^2)H(1-x)$, $\Gamma(x, y, 0) = H(1-x)$ where $H(x) \equiv \frac{1}{2}(1 + \tanh(Kx))$.

The problem is parameterized by δ, the dimensionless precursor film thickness, K, controlling the shape of the initial condition, $C = \epsilon^2\sigma^\star/S^\star$, a surface tension parameter and $D = \mu^\star D^\star/S^\star H^\star$, a dimensionless diffusivity. In what follows we assume that $\delta = 10^{-2}$, $K = 100$, $C = 10^{-3}$ and $D = 10^{-7}$. Assuming $\epsilon = 10^{-2}$, this value of C corresponds to $S^\star/\sigma^\star = 0.1$, allowing us to neglect variations in surface tension in the capillary terms; for an analysis of such effects see Krechetnikov & Homsy (2004).

In § 3 we use a finite difference method to compute y-independent solutions of (2.1) satisfying

$$h_t + Q_x = 0, \quad Q \equiv -\tfrac{1}{2}h^2\Gamma_x + \tfrac{1}{3}Ch^3h_{xxx}, \tag{2.2a}$$

$$\Gamma_t + q_x = 0, \quad q \equiv -h\Gamma\Gamma_x + \tfrac{1}{2}Ch^2\Gamma h_{xxx} - D\Gamma_x, \tag{2.2b}$$

where Q and q are fluid and surfactant fluxes. Our numerical scheme employed a fixed but spatially non-uniform grid, with grid points clustered in regions where we anticipated rapid spatial variation. We used implicit timestepping and validated convergence using grid refinement. For the simulations shown, the grid spacing varied from 10^{-4} where the film was extremely thin (regions A, II and B in figure 2) to 0.005 elsewhere. We used the same parameters as Warner *et al.* (2004*a*) but a finer computational grid; while the overall features of the flow are as they reported, we resolve some important details not described previously.

3. Drop spreading: numerical results

Figure 3(a, b) shows numerical simulations of (2.2) at late times, when the solution exhibits the structure sketched in figure 2. Figure 3(c–f) shows the evolution of some key variables which characterize the spreading process: x_1 (the location of the pressure minimum closest to $x = 0$, representing the location of the drop's effective contact line); x_2 (where the curvature in h changes at the downstream end of the ultra-thin film, representing the location of the rarefaction wave); x_3 (the leading edge of the monolayer, satisfying $\Gamma(x_3, t) = 10^{-4}$); $h_0 = h(0, t)$ (the maximum drop height) and $h_1 = h(x_1, t)$ (representative of the thickness of the ultra-thin film ahead of the contact line); surfactant concentrations $\Gamma_0 = \Gamma(0, t)$ and $\Gamma_2 = \Gamma(x_2, t)$; and surfactant gradients $k_1 = -\Gamma_x(x_1, t)$ and $k_2 = -\Gamma_x(x_2, t)$. Figure 3(a, d) illustrates the dramatic variations in film thickness between the bulk drop (where $h_0 = O(1)$, not shown in figure 3a), the precursor film thickness (where $h = \delta = 0.01$) and the thickness of the ultra-thin film ahead of the contact line (where h_1 falls to around 10^{-4}). For later reference, we also show the relationships between some of the characteristic variables (figure 3g–i).

As might be anticipated, much of the spreading is locally self-similar. We illustrate this by replotting in figure 4 the data shown in figure 3(a, b) when rescaled with suitable variables (using scalings justified in § 4 below). The data are shown to collapse in the bulk drop region (figure 4a, b, labelled I in figure 2), the contact-line region (figure 4c, d, A in figure 2), the rarefaction wave at the downstream edge of the ultra-thin film (figure 4e, f, B in figure 2) and the spreading monolayer region (figure 4g, h, III in figure 2). We now examine these self-similar structures in more detail.

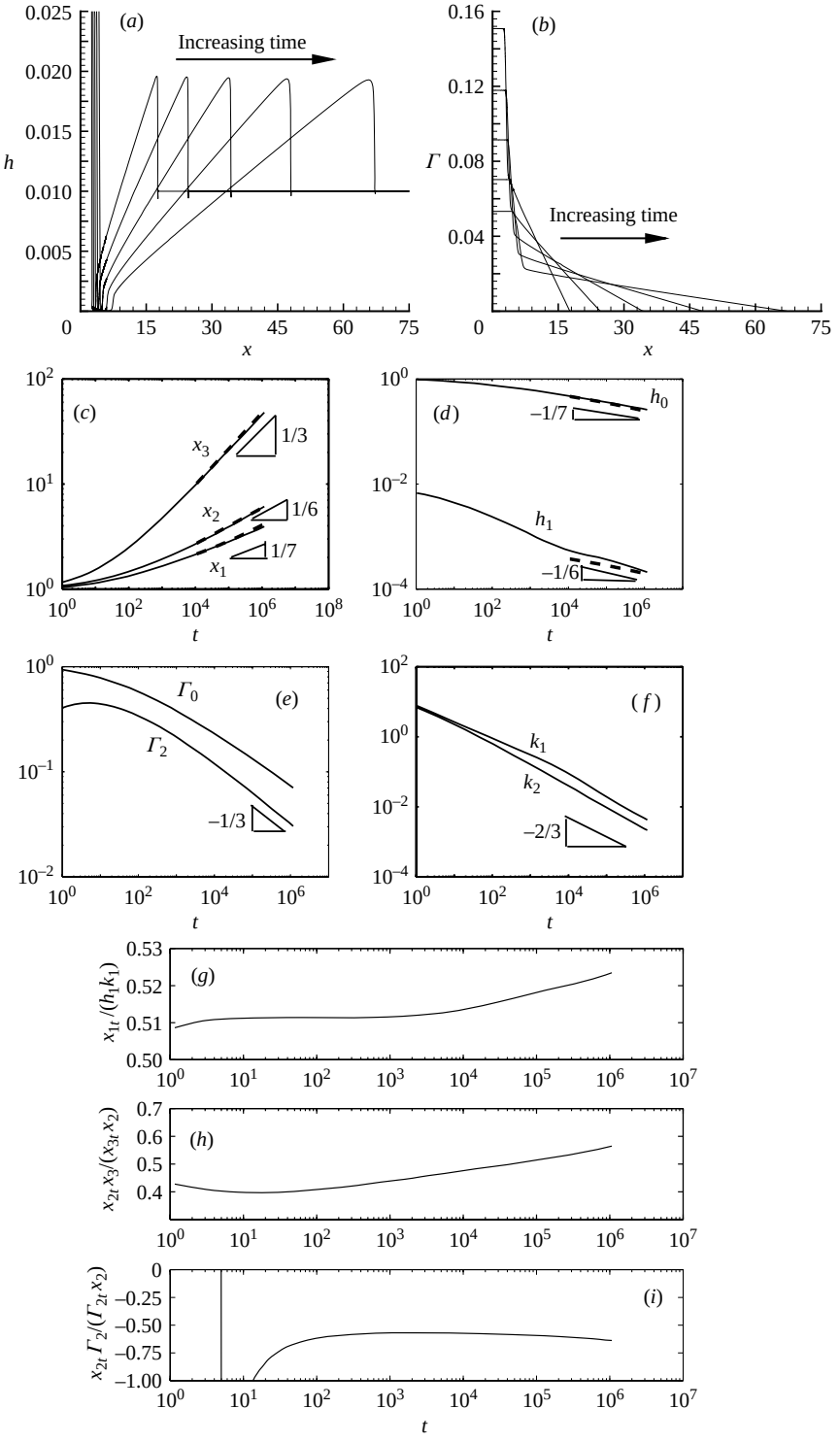

FIGURE 3. Evolution of (*a*) film thickness h (shown at heights comparable to the precursor film thickness) and (*b*) surfactant concentration Γ for $t = (0.05, 0.16, 0.45, 1, 3) \times 10^6$. (*c–f*) show evolution of key variables (defined in the text); solid lines show solutions of (2.2); dashed lines in (*c*, *d*) show solutions of (4.17). (*g–i*) show respectively $\hat{V} = x_{1t}/h_1 k_1$, $x_{2t}x_3/(x_{3t}x_2)$ and $x_{2t}\Gamma_2/(\Gamma_{2t}x_2)$ versus t.

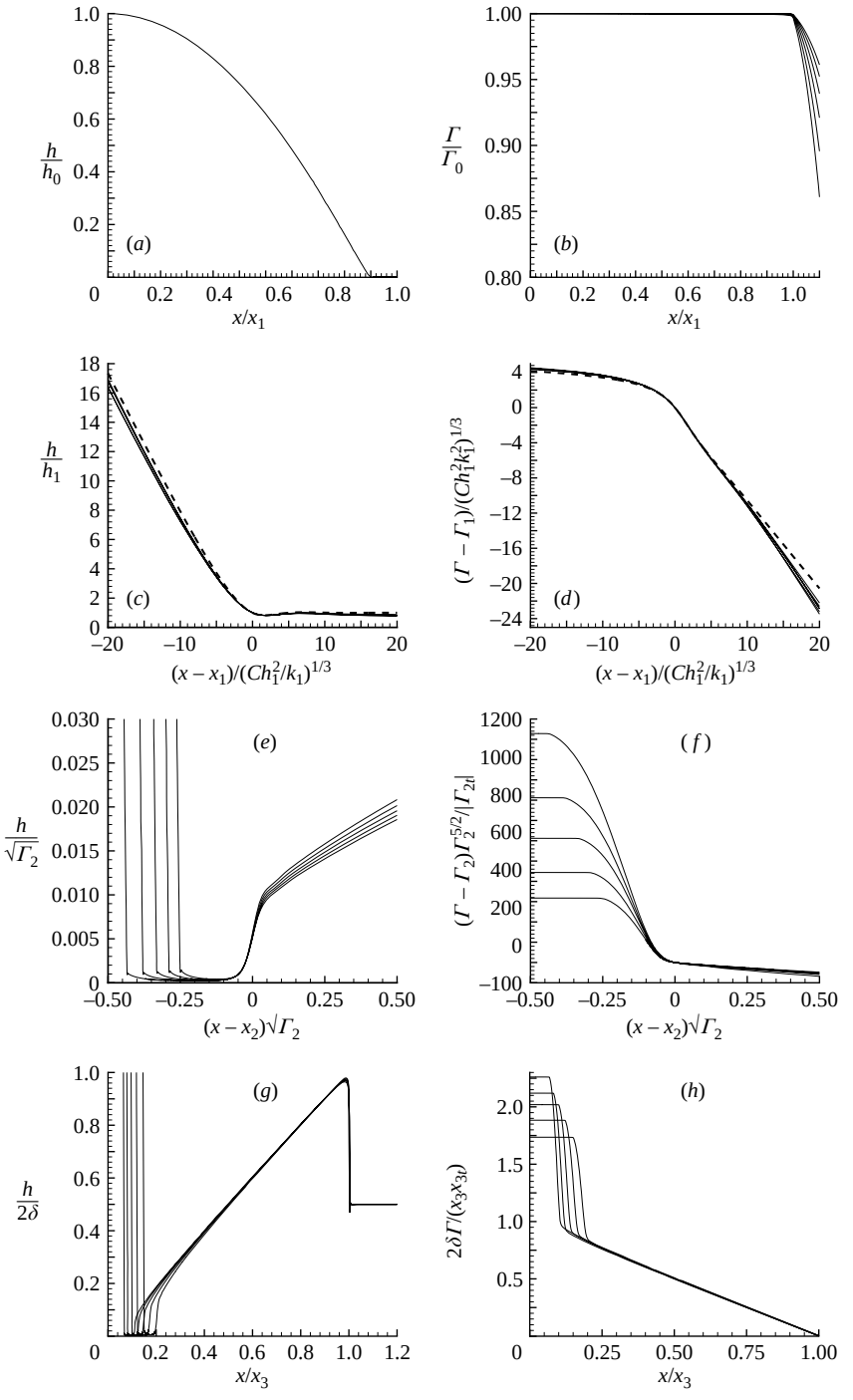

FIGURE 4. Evolution of h and Γ (a, b) in region I, (c, d) in region A, (e, f) in region II and (g, h) in region III, using data shown in figure 3(a, b). Dashed lines in (c, d) show the solution of (4.5) with $\hat{V} = 0.51$. In (d), $\Gamma_1 = \Gamma(x_1, t)$.

4. Drop spreading: asymptotic approximation

For the flow arising from the initial conditions used in our simulation, we postulate a long-time asymptotic structure consisting of six non-trivial regions, three long (I–III) and three short (A–C) (see figure 2), from which we derive an approximate ODE model ((4.17) below) describing the evolution of the system. We now discuss each region in turn, neglecting hereafter the effects of surface diffusion.

(i) *Region I.* In $0 \leqslant x < x_1(t)$ the drop is quasi-static and parabolic and the surfactant distribution is almost uniform (figure 4*a*, *b*). We therefore write $\Gamma = \Gamma_0 + \hat{\Gamma}(x,t)$, taking $|\hat{\Gamma}| \ll \Gamma_0$. To leading order in $\hat{\Gamma}/\Gamma_0$, (2.2) becomes

$$h_t = \left(\tfrac{1}{2}h^2\hat{\Gamma}_x - \tfrac{1}{3}Ch^3h_{xxx}\right)_x, \qquad 0 = \left(h\hat{\Gamma}_x - \tfrac{1}{2}Ch^2h_{xxx}\right)_x. \tag{4.1a, b}$$

Integrating (4.1*b*), applying no flux at $x=0$, gives $h\hat{\Gamma}_x = \frac{1}{2}Ch^2h_{xxx}$, and so (4.1*a*) becomes $h_t + \frac{1}{12}(h^3h_{xxx})_x = 0$, the evolution equation for a drop spreading under an immobile interface. This has the leading-order solution $h = h_0[1 - (x^2/x_1^2)]$ in $0 \leqslant x < x_1$ (as in figure 4*a*). Because there is negligible volume flux through the drop's effective contact line, the drop volume $\mathscr{V} = \frac{2}{3}h_0x_1$ remains almost constant during the motion. The effective contact angle at the edge of the bulk droplet is $\theta = -h_x(x_1-,t) = 2h_0/x_1 = 3\mathscr{V}/x_1^2$.

(ii) *Region A.* A thin transition region at $x = x_1(t)$ connects the bulk droplet to the ultra-thin film (in region II) of thickness $O(h_1) \ll h_0$. This contact-line region is controlled by competing capillary and Marangoni forces. Balancing convective and capillary fluxes in (2.2*a*), $x_{1t}h_x \sim C(h^3h_{xxx})_x$ (where $\sim$ denotes 'scales like') implies $\theta \sim (x_{1t}/C)^{1/3}$. Balancing convective and Marangoni fluxes $x_{1t}h_x \sim (h^2\Gamma_x)_x$ implies $x_{1t} \sim h_1k_1$. This gives a lengthscale for region A of $h_1/\theta \sim (Ch_1^2/k_1)^{1/3} \ll x_1$. We assume that changes in Γ across region A, of size $(k_1^2Ch_1^2)^{1/3}$, are small compared to Γ_0. We then set

$$x = x_1 + \left(Ch_1^2/k_1\right)^{1/3}\xi, \quad h = h_1H(\xi), \quad \Gamma = \Gamma_0 + \left(k_1^2Ch_1^2\right)^{1/3}G(\xi), \quad x_{1t} = h_1k_1\hat{V}. \tag{4.2}$$

Figure 4(*c*, *d*) shows how the PDE data collapse when scaled using these variables (for clarity we used $\Gamma_1 = \Gamma(x_1,t) \approx \Gamma_0$ in figure 4*d*). Assuming ξ, H, G and $\hat{V}$ are all $O(1)$, (2.2) reduces at leading order to

$$-\hat{V}H_\xi + \left(-\tfrac{1}{2}H^2G_\xi + \tfrac{1}{3}H^3H_{\xi\xi\xi}\right)_\xi = 0, \quad \left(-HG_\xi + \tfrac{1}{2}H^2H_{\xi\xi\xi}\right)_\xi = 0. \tag{4.3}$$

Integrating, applying the boundary conditions $H \to H^\infty$, $G_\xi \to G_\xi^\infty$ as $\xi \to \infty$, and imposing the conditions $H=1$ and $G_\xi = -1$ where $H_{\xi\xi\xi} = 0$ (at $\xi = 0$, by definition of x_1), we find that $H^\infty = 1$, $G_\xi^\infty = -1$ and

$$\hat{V}(1-H) + \tfrac{1}{3}H^3H_{\xi\xi\xi} = \tfrac{1}{2}(1 + H^2G_\xi), \quad \tfrac{1}{2}H^2H_{\xi\xi\xi} = 1 + HG_\xi. \tag{4.4}$$

Eliminating HG_ξ gives

$$\tfrac{1}{12}H^3H_{\xi\xi\xi} = \left(\hat{V} - \tfrac{1}{2}\right)(H-1), \quad G_\xi = (6\hat{V}-4)/H - (6\hat{V}-3)/H^2. \tag{4.5a, b}$$

We recognise (4.5*a*) as the Landau–Levich equation. The volume flux has three components: the motion of the wall (relative to this moving frame), dragging liquid into the drop; the capillary pressure gradient; and the Marangoni flux pulling liquid out of the drop. Figure 3(*g*) shows that $\frac{1}{2} < \hat{V} < \frac{2}{3}$ at large times, implying that the advancing contact line accumulates liquid more rapidly than the Marangoni flow draws liquid out of the drop; for such $\hat{V}$, (4.5*a*) has a unique solution for

which $H_{\xi\xi} \to 0$ as $\xi \to -\infty$ and $G_\xi < 0$ across region A. This solution is shown in figure 4(c, d) for $\hat{V} = 0.51$; it matches the PDE data closely. (The constant arising from integrating (4.5b) was chosen such that $G(0) = 0$.) The outer limit of the solution of (4.5a) may be written

$$H^3 = 3(12\hat{V} - 6)\xi^3[\phi_0 - \log(-\xi)] \quad (\xi \to -\infty) \tag{4.6}$$

for some constant ϕ_0. We may write the log term as $\log[(x_1 - x)/x_1] + \log[x_1/(Ch_1^2/k_1)^{1/3}]$, so that in the overlap between regions I and A, where $(Ch_1^2/k_1)^{1/3} \ll x_1 - x \ll x_1$, the latter contribution is dominant. Matching to region I, we can write the local slope θ as

$$\theta^3 = (12/C)\big(x_{1t} - \tfrac{1}{2}h_1k_1\big)\mathscr{L} \quad \text{where} \quad \mathscr{L} \equiv \log\big(k_1x_1^3/Ch_1^2\big) \gg 1. \tag{4.7}$$

Troian *et al.* (1990), Joanny (1989) and Ramé (2001) obtained expressions equivalent to (4.7) (a modification of Tanner's law), although only Ramé included a logarithmic factor.

(iii) *Region III.* Figure 4(g, h) shows that the spreading monolayer in $x_2 < x < x_3$ exhibits the self-similar structure identified in Jensen & Grotberg (1992). Assuming $h = H(\varsigma)$, $\Gamma = x_3^{-1}G(\varsigma)$ where $x = \varsigma x_3$, (2.2) becomes, with error $O(1/x_3)$,

$$x_3^2x_{3t}\varsigma H_\varsigma + \tfrac{1}{2}(H^2G_\varsigma)_\varsigma = 0, \quad x_3^2x_{3t}(\varsigma G)_\varsigma + (HGG_\varsigma)_\varsigma = 0. \tag{4.8}$$

Numerical results (figure 3c) support the assumption that $x_3^2x_{3t} = O(1)$. By imposing $H = 2\delta$ and $G = 0$ at $\varsigma = 1$, we obtain $H = 2\delta\varsigma$, $G = (x_3^2x_{3t}/2\delta)(1 - \varsigma)$. In the original variables, $h = 2\delta x/x_3$, $\Gamma = (x_{3t}/2\delta)(x_3 - x)$ in $x_2 < x < x_3$, consistent with figure 4(g, h). We now define $(h_2^\pm, k_2^\pm)$ as $\lim(h, -\Gamma_x)$ as $x \to x_2\pm$ from within regions III and II respectively, distinguishing them from the numerically determined quantities (h_2, k_2). Then to leading order, as $x \to x_2+$, writing the surface velocity at x_2 as U_2^S,

$$h_2^+ = 2\delta x_2/x_3, \quad \Gamma_2 = k_2^+(x_3 - x_2), \quad k_2^+ = x_{3t}/2\delta, \quad U_2^S = -h\Gamma_x = x_{3t}x_2/x_3. \tag{4.9a–d}$$

(iv) *Region C.* The structure of the kinematic shock near $x = x_3$ has been described in detail previously (Jensen & Grotberg 1992; Jensen & Halpern 1998; Jensen 1998). (This region is referred to as a 'convection front' by some authors.) In the parameter regime relevant here, the discontinuity in film thickness is smoothed by capillary effects and the jump in surfactant gradient is smoothed by surface diffusion, but the region remains dynamically passive. The shock speed is characteristic. Ahead of region C the film is undisturbed.

(v) *Region B.* Near $x = x_2$, between the ultra-thin film (region II) and the spreading monolayer, is an abrupt jump in film height and surfactant concentration (figure 4e, f), which we now show is smoothed via a rarefaction wave over a lengthscale long enough for capillary and diffusive effects to be negligible at leading order. To ensure continuity of surfactant flux across the region we impose $h_2^+k_2^+ = h_2^-k_2^-$, which using (4.9) implies $k_2^- = x_2x_{3t}/(h_2^-x_3)$. Continuity of volume flux in (2.2a) is ensured by the Rankine–Hugoniot condition $x_{2t} = \frac{1}{2}h_2^+k_2^+ = \frac{1}{2}x_2x_{3t}/x_3$. The validity of this assumption is tested in figure 3(h), which shows that $x_{2t}x_3/x_{3t}x_2$ remains close to 0.5 over many decades of time; the agreement is not perfect but is reasonable considering that x_2 is defined (numerically) somewhat arbitrarily (it is difficult to pinpoint the precise location of an expanding structure). We then write $x = x_2 + \zeta$, $\Gamma(x, t) = \Gamma_2(t) + \tilde{\Gamma}(\zeta, t)$ (assuming $|\tilde{\Gamma}| \ll \Gamma_2$), with Γ_2 given by (4.9a). Substitution in (2.2b) gives to leading order $(h\tilde{\Gamma}_\zeta)_\zeta = \Gamma_{2t}/\Gamma_2$. Integrating and imposing $h\tilde{\Gamma}_\zeta = -U_2^S$

at $\zeta = 0$ (see (4.9d)) gives

$$h\tilde{\Gamma}_\zeta = (\Gamma_{2t}/\Gamma_2)\zeta - U_2^S. \tag{4.10}$$

Substituting (4.10) into (2.2a), noting that $x_{2t} = \frac{1}{2}U_2^S$, gives

$$h_t - \tfrac{1}{2}(\Gamma_{2t}/\Gamma_2)\zeta h_\zeta = \tfrac{1}{2}h\Gamma_{2t}/\Gamma_2. \tag{4.11}$$

Solving (4.11) using characteristics gives $h(\zeta, t) = h^0(\zeta_0)\sqrt{\Gamma_2(t)/\Gamma_2^0}$ on $\zeta(t) = \zeta_0\sqrt{\Gamma_2^0/\Gamma_2(t)}$ for some 'initial' condition $h^0(\zeta) = h(\zeta, t_0)$, $\Gamma_2^0 = \Gamma_2(t_0)$. (Our definition of x_2 requires $h^0_{\zeta\zeta}(0) = 0$.) Thus in terms of the original variables,

$$h(x, t) = h^0\big((x - x_2)\sqrt{\Gamma_2/\Gamma_2^0}\big)\sqrt{\Gamma_2/\Gamma_2^0}, \tag{4.12}$$

showing that the film is stretched and thinned by the local Marangoni flow; figure 4(*e*) shows that h collapses under these scalings. Where regions B and III overlap, we require $h = 2\delta x/x_3$ from (4.9a). Thus at $t = t_0$, $h^0(\zeta) = (2\delta/x_3^0)(x_2^0 + \zeta)$, where $x_2(t_0) = x_2^0$ and $x_3(t_0) = x_3^0$; subsequently

$$h(x, t) = \big(2\delta/x_3^0\big)\left(x_2^0 + (x - x_2)\sqrt{\Gamma_2/\Gamma_2^0}\right)\sqrt{\Gamma_2/\Gamma_2^0}. \tag{4.13}$$

To ensure that this matches to $2\delta x/x_3$ we require

$$\frac{x_3}{x_3^0} = \frac{\Gamma_2^0}{\Gamma_2}, \quad \frac{x_2}{x_2^0} = \sqrt{\Gamma_2^0/\Gamma_2}, \quad \text{i.e.} \quad \frac{2x_{2t}}{x_2} = \frac{x_{3t}}{x_3} = -\frac{\Gamma_{2t}}{\Gamma_2}, \tag{4.14a–c}$$

consistent with the shock condition assumed above and figure 3(*i*), which shows that (4.14c) is approximately satisfied at large times. Integrating (4.10) using (4.14) gives

$$\Gamma(x, t) = \Gamma_2(t) + \frac{\Gamma_{2t}}{\Gamma_2}\int_{x_2}^{x} \frac{x}{h}\,\mathrm{d}x, \tag{4.15}$$

which ensures matching with (4.9b). Figure 4(*f*) shows that Γ collapses under the scalings $\zeta \sim 1/\sqrt{\Gamma_2}$, $h \sim \sqrt{\Gamma_2}$ and $\tilde{\Gamma} \sim \Gamma_{2t}/\Gamma_2^{5/2}$ consistent with (4.13) and (4.15). At the trailing edge of the rarefaction wave ($x < x_2$) we assume $h^0(\zeta) \to \mathscr{H} \ll 1$ as $\zeta \to -\infty$, where $\mathscr{H}$ is determined by an earlier transient flow. Subsequently, $h_2^- = \mathscr{H}\sqrt{\Gamma_2/\Gamma_2^0}$ from (4.13), implying $h_2^- = \mathscr{H}x_2^0/x_2$.

(vi) *Region II.* In $x_1 < x < x_2$ the film is ultra-thin and the Marangoni volume flux (proportional to h^2) is consequently very small, although the surfactant flux is significant. Two approaches may be taken to describe this region. First, one may set $h(x, t) = H(\upsilon)/x_2$, $\Gamma(x, t) = \Gamma_2 + 2x_2^2x_{2t}G(\upsilon)$ where $\upsilon = x/x_2$, assuming that at large times $x_2^2x_{2t} \ll \Gamma_2$ (a condition that is asymptotic since, according to figure 3(*c*, *e*), $x_2^2x_{2t} \sim t^{-1/2}$ and $\Gamma_2 \sim t^{-1/3}$ as $t \to \infty$). Then to leading order (2.2) becomes $0 = (\upsilon H + H^2G_\upsilon)_\upsilon$, $(HG_\upsilon)_\upsilon = -1$. Integrating, and using the matching condition $HG_\upsilon \to -1$ as $\upsilon \to 1-$, we deduce $HG_\upsilon = -\upsilon$ for $(x_1/x_2) < \upsilon < 1$, implying a linear surface velocity across region II. Both the fluid and surfactant transport equations are then satisfied to leading order, implying that the film distribution $H(\upsilon)$ throughout region II is determined by the initial conditions. Strong stretching of the interface leads to severe film thinning and the flow here has a hyperbolic character. Since $h(x_2-, t) = \mathscr{H}x_2^0/x_2$, we require $H = H^0(\upsilon)$ for some H^0 where $H^0(1) = \mathscr{H}x_2^0$; G can then be determined by integration using $G(1) = 0$. If, for example, $H(\upsilon) = \mathscr{H}x_2^0/\upsilon$, then $h = \mathscr{H}x_2^0/x$, implying that the film's shape is effectively frozen in region II while the contact line advances over it.

Unfortunately, over the timescales accessible to computation the assumption $\Gamma_2 \gg x_2^2x_{2t}$ is not well-satisfied (the changes in Γ across region II remain appreciable, see

for example figure 4*h*) and a second approach using an approximate solution proves more useful. Since the volume flux in region II is very small, we assume the film takes the frozen distribution described above, so that $h_1 = \mathscr{H} x_2^0/x_1$ for some $\mathscr{H}$. We then assume that the surfactant concentration is large enough for the surfactant distribution to reach steady state across this region so that the surfactant flux is uniform (in practice there is approximately up to 20 % variation over the times shown in figure 3). Thus $h_1\Gamma_0 k_1 = h_2^- \Gamma_2 k_2^- = -(\mathscr{H} x_2^0/x)\Gamma\Gamma_x$, from which we find that

$$\Gamma^2 = \Gamma_2^2 + \Gamma_2 k_2^- \left(x_2^2 - x^2\right)/x_2, \tag{4.16}$$

implying $\Gamma_0^2 = \Gamma_2^2 + \Gamma_2 k_2^- (x_2^2 - x_1^2)/x_2$.

(vii) *ODE model.* We now evaluate the total mass of surfactant in the monolayer,

$$\mathscr{M} = \int_0^\infty \Gamma \,\mathrm{d}x = \Gamma_0 x_1 + \int_{x_1}^{x_2} \Gamma \,\mathrm{d}x + \tfrac{1}{4} x_{3t}(x_3 - x_2)^2/\delta, \tag{4.17a}$$

where Γ in the integral satisfies (4.16). This provides an evolution equation for x_3. With the evolution equation for x_1 provided by (4.7), which we may write as

$$x_{1t} = \left[9\mathscr{V}^3 C/4\mathscr{L} x_1^6\right] + \tfrac{1}{2} h_1 k_1, \tag{4.17b}$$

we now have a closed system since, using expressions derived above for h_1, x_2, Γ_2, h_2^-, k_2^- and Γ_0, all the variables may be described in terms of $x_1(t)$, $x_3(t)$, parameters $\mathscr{V}$, $\mathscr{M}$, C and δ and integration constants x_1^0, x_2^0, x_3^0, Γ_2^0 and $\mathscr{H}$.

The PDE simulations used $\mathscr{M} = 1$, $\mathscr{V} = \frac{2}{3}$. Fitting x_1^0, x_2^0, x_3^0 and Γ_2^0 to PDE data at $t_0 = 10^4$, and setting $\mathscr{H} = 3 \times 10^{-4}$, (4.17) provides a good approximation for behaviour in $t > 10^4$ (figure 3*c*, *d*). The long-lived influence of the initial conditions and subsequent transient flows in region II prohibits a uniformly asymptotic approximation, and limits the accuracy of predictions of $h_1(t)$, but nevertheless illustrates a critically important feature of the spreading dynamics. Once $x_1 \ll x_2 \ll x_3$, further simplification is possible: the majority of the surfactant is contained in region III, so that (from (4.17*a*)) $M \approx x_3^2 x_{3t}/(4\delta)$, implying $x_3 \propto t^{1/3}$, $x_2 \propto t^{1/6}$ and $\Gamma_2 \propto t^{-1/3}$ (from (4.14)); a balance of terms in (4.17) suggests $x_1 \propto t^{1/7}$ (with at least a logarithmic correction) and volume conservation in region I then implies $h_0 \propto t^{-1/7}$. These scalings are all borne out by PDE solutions in figure 3(*c*–*f*). Our crude approximation for region II suggests $h_1 = \mathscr{H} x_2^0/x_1 \propto t^{-1/7}$, although the PDE data are closer to $t^{-1/6}$ (figure 3*d*), again reflecting our imperfect knowledge of the local effect of transient dynamics.

5. Stability to transverse perturbations

Having captured to a reasonable level of accuracy the structure and dynamics of the spatially one-dimensional flow, we now investigate its stability to small-amplitude disturbances. Linear stability analysis of the entire time-dependent flow (Warner *et al.* 2004*a*) showed that growing disturbances are initially confined to the neighbourhood of the drop's contact line. We therefore focus on region A, perturbing the quasi-steady Landau–Levich solution satisfying (4.5), looking for disturbances with spanwise wavenumber k. By treating the basic state as quasi-steady during the evolution of disturbances, its weak algebraic time-dependence is captured parametrically through $\hat{V}$.

The scaling (4.2) with $t = (C/k_1^4 h_1)^{1/3}\tau$, $y = (Ch_1^2/k_1)^{1/3}\eta$ reduces (2.1) in region A (neglecting surface diffusion) to

$$H_\tau - \hat{V} H_\xi = \left[\tfrac{1}{2} H^2 G_\xi - \tfrac{1}{3} H^3 (\nabla^2 H)_\xi\right]_\xi + \left[\tfrac{1}{2} H^2 G_\eta - \tfrac{1}{3} H^3 (\nabla^2 H)_\eta\right]_\eta, \tag{5.1a}$$

$$0 = \left[H G_\xi - \tfrac{1}{2} H^2 (\nabla^2 H)_\xi\right]_\xi + \left[H G_\eta - \tfrac{1}{2} H^2 (\nabla^2 H)_\eta\right]_\eta. \tag{5.1b}$$

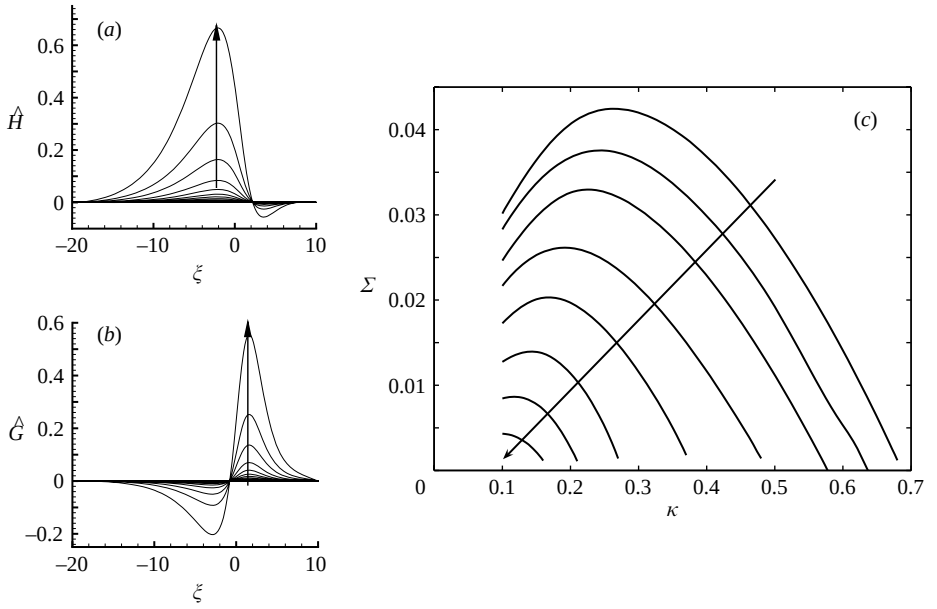

FIGURE 5. (a, b) Solutions of (5.2) for $\kappa = 0.3$ and $\hat{V} = 0.52$; arrows show increasing times between 1 and 200. (c) Large-time growth rate Σ versus wavenumber κ for $\hat{V} = 0.52, 0.53, \ldots, 0.59$ (the arrow shows $\hat{V}$ increasing).

Setting $(H, G) = (H_s, G_s) + \beta(\hat{H}, \hat{G})\mathrm{e}^{i\kappa\eta}$ and $\kappa = (Ch_1^2/k_1)^{1/3}k$, we recover at leading order in $\beta \ll 1$ the steady solution (4.3) (now denoted with a subscript s). The linearized unsteady disturbances satisfy

$$\hat{H}_\tau - \hat{V}\hat{H}_\xi = \left[\tfrac{1}{2}H_s^2\hat{G}_\xi + H_sG_{s\xi}\hat{H} - \tfrac{1}{3}H_s^3\left(\partial_\xi^2 - \kappa^2\right)\hat{H}_\xi - H_s^2H_{s\xi\xi\xi}\hat{H}\right]_\xi - \tfrac{1}{2}\kappa^2H_s^2\hat{G} + \tfrac{1}{3}\kappa^2H_s^3\left(\partial_\xi^2 - \kappa^2\right)\hat{H}, \quad (5.2a)$$

$$0 = \left[H_s\hat{G}_\xi + G_{s\xi}\hat{H} - \tfrac{1}{2}H_s^2\left(\partial_\xi^2 - \kappa^2\right)\hat{H}_\xi - H_sH_{s\xi\xi\xi}\hat{H}\right]_\xi - \kappa^2H_s\hat{G} + \tfrac{1}{2}\kappa^2H_s^2\left(\partial_\xi^2 - \kappa^2\right)\hat{H}. \quad (5.2b)$$

We solved (5.2) numerically by timestepping, using a uniform finite-difference grid on a domain $-50 \leqslant \xi \leqslant 50$, tracking the evolution of localized disturbances (initially $\hat{H} = \hat{G} = 0.001\exp(-10\xi^2)$). The evolution depends on the prescribed wavenumber κ and the contact-line speed (parameterized by $\hat{V}$). Figure 5(a, b) shows how, under suitable conditions, disturbances can grow rapidly: perturbations to $\hat{H}$ are larger behind the contact line (in $\xi < 0$), while perturbations to $\hat{G}$ are larger ahead of it ($\xi > 0$), features identified previously by Warner *et al.* (2004*a*). At large times (for $t \gtrsim 10^3$) the growth is approximately exponential (with $\hat{H}, \hat{G} \propto \exp\Sigma\tau$). The computed growth rate Σ is shown in figure 5(c) as a function of κ for fixed values of $\hat{V}$; the shape of the dispersion relation resembles that obtained by Warner *et al.* (2004*a*) using their quasi-steady-state approximation. For small κ, growing disturbances ultimately reached the left-hand boundary of the domain (where the base state is non-uniform); growth rates were then sensitive to the size of the domain chosen. This prevented us from computing reliable solutions for $\kappa < 0.1$. However, the simulations demonstrate convincingly that, at least for $\hat{V}$ just above 0.5, the most unstable mode has wavenumber comparable to the width of region A, that

increases in the parameter $\hat{V}$ (representing the ratio of the advective to Marangoni fluxes through the contact line) that can occur during spreading (see figure 3*g*) have a stabilizing effect, and that sufficiently short-wavelength disturbances are stable.

Further insight may be gained by analysing the eigenmode associated with the translation invariance of the basic state, which forms part of the discrete spectrum of the linear operator in (5.2). As shown in the Appendix, for $\kappa \ll 1$ this mode has growth rate

$$\Sigma = \kappa[2 - 3\hat{V} + O(1/\mathscr{L}_s)] + o(\kappa), \tag{5.3}$$

where $\mathscr{L}_s$ is as defined by $\mathscr{L}$ in (4.7). Despite being only logarithmically accurate, this approximation corroborates our observation that disturbances grow more slowly as the contact-line speed increases, and the predicted cutoff at which Σ/κ becomes negative as $\kappa \to 0+$ (namely $\hat{V} = \frac{2}{3} + O(1/\mathscr{L}_s)$) is consistent with figure 5(*c*), at least to within the limited accuracy of the asymptotic and numerical approaches. To improve the accuracy of both techniques in this regime requires fuller consideration of the dynamics in the bulk droplet and a more thorough analysis of the spectra of (5.2). However, the long-wave asymptotic analysis in the Appendix clearly reveals a physical mechanism leading to the fingering instability (that differs somewhat from the qualitative scenario proposed by Warner *et al.* 2004*a*). A foward perturbation of the contact line compresses the monolayer in region II and increases the surfactant gradient ahead of the drop (without altering the film height, consistent with figure 5(*a*); see (A 3)) but reduces the contact angle of the drop (without generating stabilizing capillary pressure gradients to leading order; likewise Marangoni effects are weak because the monolayer can equilibrate where the film is thick, consistent with figure 5(*b*), see (A 5)). The two effects compete to displace the contact line further through (4.7), with the elevated Marangoni flux winning, particularly at low contact-line speeds, hence generating an instability.

6. Discussion

We have used simulation and asymptotic analysis to describe the late-time spreading dynamics of a two-dimensional surfactant-laden drop over a precursor film. Our results give insights into some important physical mechanisms that were not accessible from previous computational studies. An over-riding feature of this problem, in terms of predicting spreading rates and subsequent instabilities, and distinguishing it from classical drop-spreading problems, is the long-lived influence of the initial conditions. In particular, we have shown how the structure of the ultra-thin film immediately ahead of the drop's effective contact line (region II in figure 2; see also figure 4*e*, *f*) depends explicitly on earlier transient flows. In constructing our ODE model of planar spreading, this required us to make *ad hoc* estimates of the film thickness h_1 and surfactant gradient k_1 immediately ahead of the contact line (§ 4), and also to take starting values of other parameters from PDE simulations. Thereafter, however, our model (4.17) provided a good approximation of the late-time spreading dynamics (see figure 3*c*, *d*). We showed how, for the particular initial conditions chosen, a rarefaction wave arises across which the film thickness jumps dramatically (region B in figure 2; see also figure 1). This structure is reminiscent of various shock-like structures leading to severe film thinning in thermally driven thin-film flows (e.g. Bertozzi, Münch & Shearer 1999; Münch 2003), although the coupling of the surfactant distribution to the flow adds extra complexity to the present problem and prevents direct analogies from being drawn. A particularly striking demonstration of the importance of initial

conditions comes from further simulations (not shown) in which we assumed both the initial surfactant distribution and the film thickness to be parabolic (rather than taking Γ to be uniform across the drop). In this case, a wholly different flow structure arises, with regions II and B absent and the drop's contact line (region A) connecting directly to the spreading monolayer in region III. Warner *et al.* (2004*a*) demonstrated how changing other parameters, such as the precursor film thickness, can have similarly striking effects on the long-time dynamics. These observations raise challenging mathematical questions concerning the conditions necessary for the formation of a rarefaction wave and the associated ultra-thin film, and also emphasize the importance in experimental studies of using well-characterized and reproducible initial conditions.

Fundamental to both the drop's spreading rate and subsequent instabilities is the relationship between contact angle and contact-line speed. It is instructive to re-express the analogue we derived of Tanner's law (4.7) in unscaled, dimensional terms

$$\theta^{\star 3} = 12\big(Ca - \tfrac{1}{2}h_1^\star/X^\star\big)\log\big(x_1^{\star 3}/h_1^{\star 2}X^\star\big), \tag{6.1}$$

where $Ca = \mu^\star x_{1t^\star}^\star/\sigma^\star$ is the capillary number associated with the moving contact line and $X^\star = \sigma^\star/(\mathrm{d}\sigma^\star/\mathrm{d}x^\star)$ can be interpreted as the lengthscale over which the surface tension varies ahead of the contact line. The logarithmic factor in (6.1) includes the ratio of the drop width $x_1^\star(t^\star)$ to $(h_1^{\star 2}X^\star)^{1/3}$, the width of region A (where $h_1^\star$ is the dimensional thickness of the film immediately ahead of the contact line). As explained above, $X^\star$ and $h_1^\star$ have complex dependence both on the initial conditions and on the governing parameters of the problem, making direct comparison with experiment difficult. However, our model (4.17) illustrates the connection between the dynamics of the drop and that of the monolayer, and identification of relationships such as (6.1) should facilitate further extensions of the present model to account for experimentally significant effects such as an axisymmetric geometry, surfactant solubility (see Warner, Craster & Matar 2004*b*), intermolecular forces, and so on.

Warner *et al.* (2004*a*), who examined the stability of the entire flow numerically, showed how growing disturbances of the spreading drop are confined to the neighbourhood of the advancing contact line. Here we have identified a substantially simpler problem which captures much of the dominant dynamics, by restricting attention to perturbations confined to region A in figure 2. By perturbing a solution of the Landau–Levich equation (4.5), we showed (figure 5) that the most rapidly growing linearized disturbances have a wavelength comparable to $(h_1^{\star 2}X^\star)^{1/3}$, the width of region A, and that the growth rate is dependent on the relative speed of the contact line (represented by Ca in (6.1)) and the speed at which Marangoni fluxes pull liquid out through the contact line (represented by the ratio $h_1^\star/2X^\star$), so that faster contact line speeds (or weaker Marangoni fluxes) are stabilizing (provided $Ca > h_1^\star/2X^\star$). Furthermore, we identified (in the Appendix) the singular structure in the long-wavelength limit of the discrete mode associated with the translation invariance of the base state, which illustrates explicitly a mechanism leading to instability. (It is notable that while (5.2) is satisfied by the translation mode to $O(\kappa^2)$, the boundary condition (6.1) is perturbed at $O(\kappa)$.) Perturbations generate long-range disturbances in the monolayer concentration ahead of the contact line, and in the film thickness behind it, which lead to the growth of disturbances at a rate given approximately by (5.3), which in dimensional terms becomes $\Sigma^\star \approx (\sigma^\star k^\star/\mu^\star)(2h_1^\star/X^\star - 3Ca)$, where $k^\star$ is the spanwise wavenumber. Going to the following order, the dispersion relation for this mode may well be of the form $\Sigma \approx a\kappa - b\kappa^3$ for constants a and b,

which supports the proposed analogy with viscous fingering in porous media or a Hele-Shaw cell (Troian *et al.* 1990). However, the analogy is imperfect. For example, since Ca is comparable to $(h_1^\star/X^\star)$ (see (6.1)), the wavelength of disturbances scales with $h_1^\star Ca^{-1/3}$, whereas for viscous fingering problems the wavelength typically scales like $Ca^{-1/2}$ (Homsy 1987). Our simulations also showed that growing long-wave disturbances can extend into the bulk drop, indicating that the bounded eigenmodes associated with the discrete spectrum of (5.2) fail to capture the full dynamics. A more detailed analysis, examining transient growth and the nature of the continuous spectrum, is warranted. The relationship between the present instability and finger formation in a meniscus advancing over a precursor film in a Hele-Shaw cell (Chan & Liang 1997) also deserves further investigation.

Finally, it is striking how the complex competition between Marangoni and capillary forces leads to an order-of-magnitude difference between the rate of spreading of the surfactant and the bulk droplet (compare x_1 and x_3 in figure 3*c*). This places limitations on the use of surfactant as a vehicle for enhanced delivery of a solute (for example a drug in an inhaled aerosol droplet), because the solute would be largely confined to the bulk droplet by severe film thinning at the drop's contact line. This effect can be reduced by lowering initial surfactant gradients as much as possible.

This work was supported in part by Wellcome Trust grant 061142 and EPSRC JREI Scheme GR/R08292/01.

Appendix. The long-wavelength limit of the translation mode

We examine instabilities with wavelength intermediate between the width of region A and regions I and II and assume exponential time-dependence so that $\hat{H}_\tau$ in (5.2*a*) becomes $\Sigma\hat{H}$. When $\kappa \ll 1$ we assume that the eigenmode associated with the translation invariance of the basic state has a three-region structure: an inner region, in which $\xi = O(1)$, in which the contact line is displaced sideways; and two outer regions with lengthscales $O(1/\kappa)$. We suppose that the drop's effective contact line (when viewed from the outer regions) lies along $\xi = \beta E$, so that in the inner region the leading-order solution of (5.2) is $\Sigma = 0$, $\hat{H} = -H_{s\xi}$, $\hat{G} = -G_{s\xi}$. Thus to leading order, at the outer limits of the inner region, we have

$$H \sim -\hat{\theta}_s(\xi - \beta E) \quad (\xi \to -\infty), \qquad G \sim -(\xi - \beta E) \quad (\xi \to \infty), \tag{A 1a, b}$$

where $E \equiv \exp(\mathrm{i}\kappa\eta + \Sigma\tau)$. We now show how the perturbation to G in (A 1*b*) affects the surfactant gradient $\hat{G}_\xi$ ahead of the contact line, and how the perturbation of H in (A 1*a*) affects the contact angle behind the contact line.

To describe the outer regions we rescale with $\xi = z/\kappa$, $\hat{G} = \bar{G}/\kappa$, $\Sigma = \kappa\bar{\Sigma}$ (anticipating $\bar{\Sigma} = O(1)$), so that (5.2) becomes

$$\bar{\Sigma}\hat{H} - \hat{V}\hat{H}_z = \left[\tfrac{1}{2}H_s^2\bar{G}_z + H_sG_{s\xi}\hat{H} - \tfrac{1}{3}\kappa^3H_s^3\left(\partial_z^2 - 1\right)\hat{H}_z - H_s^2H_{s\xi\xi\xi}\hat{H}\right]_z - \tfrac{1}{2}H_s^2\bar{G} + \tfrac{1}{3}\kappa^3H_s^3\left(\partial_z^2 - 1\right)\hat{H}, \tag{A 2a}$$

$$0 = \left[H_s\bar{G}_z + G_{s\xi}\hat{H} - \tfrac{1}{2}H_s^2\kappa^3\left(\partial_z^2 - 1\right)\hat{H}_z - H_sH_{s\xi\xi\xi}\hat{H}\right]_z - H_s\bar{G} + \tfrac{1}{2}\kappa^3H_s^2\left(\partial_z^2 - 1\right)\hat{H}. \tag{A 2b}$$

Ahead of the contact line, where $H_s \approx 1$ and $G_{s\xi} \approx -1$, we require $\hat{H} = o(1)$, $\bar{G} = o(z)$. With error $O(\kappa^3)$, (A 2) becomes $\bar{\Sigma}\hat{H} - \hat{V}\hat{H}_z = [\tfrac{1}{2}\bar{G}_z - \hat{H}]_z - \tfrac{1}{2}\bar{G}$, $0 = [\bar{G}_z - \hat{H}]_z - \bar{G}$,

which reduces to $\bar{\Sigma}\hat{H} = (\hat{V} - \frac{1}{2})\hat{H}_z$, $\bar{G}_{zz} - \bar{G} = \hat{H}_z$. Thus $\hat{H} = \hat{H}_0 \exp(\bar{\Sigma} z/(\hat{V} - \frac{1}{2}))$ for some $\hat{H}_0$. For $\bar{\Sigma} > 0$ and $\hat{V} > \frac{1}{2}$, we require $\hat{H}_0 = 0$ for perturbations to remain bounded as $z \to \infty$ (the contact line moves faster than any growing disturbances to the ultra-thin film). Thus $\bar{G} = \hat{G}_0 \exp(-z)$ for some $\hat{G}_0$. To match with (A 1*a*, *b*) we take $\hat{G}_0 = \kappa$. Thus towards the contact line, as $z \to 0+$, $\hat{H} = 0$ and

$$G \sim -(\xi - \beta E) - \kappa \beta E \xi, \tag{A 3}$$

showing that a forward perturbation of the contact line ($\beta E > 0$) increases the concentration gradient downstream without changing the film thickness (confirming an assumption made by Troian *et al.* 1990).

Behind the contact line, we recall from (4.5)–(4.7) that the quasi-steady basic state satisfies $H_s^2 H_{s\xi\xi\xi} \approx 12(\hat{V} - \frac{1}{2})$, $H_s G_{s\xi} \approx 6\hat{V} - 4$ and $H_s \approx -\hat{\theta}_s \xi$, where $\hat{\theta}_s^3 = (12\hat{V} - 6)\mathscr{L}_s$ and $\mathscr{L}_s \gg 1$. This is the overlap between regions A and I, where H_s is locally linear to leading order. To get a sensible balance of terms, we write $\hat{H} = \hat{\theta}_s \tilde{H}$, $\hat{G} = \kappa \hat{\theta}_s^2 \tilde{G}$ (concentration fluctuations can be smaller behind the contact line, where the film is deeper, than ahead of it, where the film is thin, for Marangoni fluxes to balance convective fluxes). Equation (A 2) reduces to

$$\bar{\Sigma}\tilde{H} + \tilde{H}_z(5\hat{V} - 2) = \hat{\theta}_s^3 \left[\tfrac{1}{2} D_2 \tilde{G} + \tfrac{1}{3} D_3 D_0 \tilde{H}\right], \tag{A 4a}$$

$$(\tilde{H}/z)_z(6\hat{V} - 2) \ = \hat{\theta}_s^3 \left[D_1 \tilde{G} + \tfrac{1}{2} D_2 D_0 \tilde{H}\right], \tag{A 4b}$$

where $D_n \equiv \partial_z z^n \partial_z - z^n$ for $n = 0, 1, 2, \ldots$. A WKB analysis for $z \to -\infty$ reveals the solution $\tilde{G} = 0$, $\tilde{H} \propto \mathrm{e}^z$ (plus more rapidly decaying solutions of the form $H \propto G \propto z^{-1/2}\mathrm{e}^z \cos(\frac{1}{2}\sqrt{3}\log z + C)$). To leading order in $\hat{\theta}_s^{-3} = O(1/\mathscr{L}_s) \ll 1$, the former mode satisfies (A 4) for $z = O(1)$. To match with (A 1*a*) we require $\tilde{H}(0) = 1$, and so $\tilde{H} = \mathrm{e}^z$. Thus with logarithmic accuracy

$$H \sim -\hat{\theta}_s(\xi - \beta E) + \kappa \hat{\theta}_s \beta E \xi, \tag{A 5}$$

showing that a forward perturbation of the contact line ($\beta E > 0$) leads to a reduction in the contact angle of the drop upstream, without the generation of pressure gradients.

We now return to the inner region to obtain a solvability condition relating (A 3) to (A 5). We write $\hat{H} = -H_{s\xi} + \kappa \hat{H}_1$, $\hat{G} = -G_{s\xi} + \kappa \hat{G}_1$ and impose matching conditions $\hat{H}_1 \to 0$ and $\hat{G}_{1\xi} \to -\xi$ as $\xi \to \infty$, and $\hat{H}_{1\xi} \to \hat{\theta}_s$ as $\xi \to -\infty$. With error $O(\kappa^2)$, (5.2) becomes

$$-\bar{\Sigma} H_{s\xi} - \hat{V}\hat{H}_{1\xi} = \left[\tfrac{1}{2} H_s^2 \hat{G}_{1\xi} + H_s G_{s\xi} \hat{H}_1 - \tfrac{1}{3} H_s^3 \hat{H}_{1\xi\xi\xi} - H_s^2 H_{s\xi\xi\xi} \hat{H}_1\right]_\xi, \tag{A 6a}$$

$$0 = \left[H_s \hat{G}_{1\xi} + G_{s\xi} \hat{H}_1 - \tfrac{1}{2} H_s^2 \hat{H}_{1\xi\xi\xi} - H_s H_{s\xi\xi\xi} \hat{H}_1\right]_\xi. \tag{A 6b}$$

We integrate and apply the downstream matching conditions (A 3) to give

$$\bar{\Sigma}(1 - H_s) - \hat{V}\hat{H}_1 = \tfrac{1}{2} H_s^2 \hat{G}_{1\xi} + \tfrac{1}{2} + H_s G_{s\xi} \hat{H}_1 - \tfrac{1}{3} H_s^3 \hat{H}_{1\xi\xi\xi} - H_s^2 H_{s\xi\xi\xi} \hat{H}_1, \tag{A 7a}$$

$$0 = H_s \hat{G}_{1\xi} + 1 + G_{s\xi} \hat{H}_1 - \tfrac{1}{2} H_s^2 \hat{H}_{1\xi\xi\xi} - H_s H_{s\xi\xi\xi} \hat{H}_1. \tag{A 7b}$$

For $\xi \to -\infty$, (A 7) becomes at leading order

$$-\bar{\Sigma} H_s + (5\hat{V} - 2)\hat{H}_1 = \tfrac{1}{2} H_s^2 \hat{G}_{1\xi} - \tfrac{1}{3} H_s^3 \hat{H}_{1\xi\xi\xi}, \tag{A 8a}$$

$$(6\hat{V} - 2)\hat{H}_1 = H_s^2 \hat{G}_{1\xi} + H_s - \tfrac{1}{2} H_s^3 \hat{H}_{1\xi\xi\xi}. \tag{A 8b}$$

We eliminate $\hat{G}_{1\xi}$ to obtain $-\bar{\Sigma} H_s + (2\hat{V} - 1)\hat{H}_1 = -\frac{1}{2} H_s - \frac{1}{12} H_s^3 \hat{H}_{1\xi\xi\xi}$. The matching condition $\hat{H}_1 \sim \hat{\theta}_s \xi$ implies that locally $\hat{H}_1 \approx -H_s$, from which we deduce

$\bar{\Sigma} = 2 - 3\hat{V} + O(1/\mathscr{L}_s)$ (and thus (5.3)), a result that can also be derived directly by assuming that (4.7) applies across the inner region.

REFERENCES

Afsar-Siddiqui, A. B., Luckham, P. F. & Matar, O. K. 2003*a* Unstable spreading of aqueous anionic surfactant solutions on liquid films. Part 1. Sparingly soluble surfactant. *Langmuir* **19**, 696–702.

Afsar-Siddiqui, A. B., Luckham, P. F. & Matar, O. K. 2003*b* Unstable spreading of aqueous anionic surfactant solutions on liquid films. Part 2. Highly soluble surfactant. *Langmuir* **19**, 703–708.

Afsar-Siddiqui, A. B., Luckham, P. F. & Matar, O. K. 2003*c* The spreading of surfactant solutions on thin liquid films. *Adv. Colloid Interface Sci.* **106**, 183–236.

Bertozzi, A. L. & Brenner, M. P. 1997 Linear stability and transient growth in driven contact lines. *Phys. Fluids* **9**, 530–539.

Bertozzi, A. L., Münch, A. & Shearer, M. 1999 Undercompressive shocks in thin film flows. *Physica* D **134**, 431–464.

Borgas, M. S. & Grotberg, J. B. 1988 Monolayer flow on a thin-film. *J. Fluid. Mech.* **193**, 151–170.

Cachile, M., Schneemilch, M., Hamraoui A. & Cazabat, A. M. 2002 Films driven by surface tension gradients. *Adv. Colloid Interface Sci.* **96**, 59–74.

Chan, K. Y. & Borhan, A. 2005 Surfactant-assisted spreading of a liquid drop on a smooth solid surface. *J. Colloid Interface Sci.* **287**, 233–248.

Chan, C. K. & Liang, N. Y. 1997 Observations of surfactant driven instability in a Hele-Shaw cell. *Phys. Rev. Lett.* **79**, 4381–4384.

Chesters, A. K. & Elyousfi A. B. A. 1998 The influence of surfactants on the hydrodynamics of surface wetting – I. The nondiffusing limit. *J. Colloid Interface Sci.* **207**, 20–29.

Churaev, N. V., Esipova, N. E., Hill, R. M., Sobolev, V. D., Starov, V. M. & Zorin, Z. M. 2001 The superspreading effect of trisiloxane surfactant solutions. *Langmuir* **17**, 1338–1348.

Clay, M. A. & Miksis, M. J. 2004 Effects of surfactant on droplet spreading. *Phys. Fluids* **16**, 3070–3078.

Cox, R. G. 1986 The dynamics of the spreading of liquids on a solid surface. Part 2. Surfactants. *J. Fluid Mech.* **168**, 195–220.

Daniels, C. B. 2001 The comparative biology of pulmonary surfactant: past, present and future. *Comp. Biochem. Physiol.* A *Mol. Integr. Physiol.* **129**, 9–36.

Eggers, J. & Stone, H. A. 2004 Characteristic lengths at moving contact lines for a perfectly wetting fluid: the influence of speed on the dynamic contact angle. *J. Fluid Mech.* **505**, 309–321.

Fischer, B. J. & Troian, S. M. 2003*a* Growth and decay of localized disturbances on a surfactant-coated spreading film. *Phys. Rev.* E **67**, 016309.

Fischer, B. J. & Troian, S. M. 2003*b* Thinning and disturbance growth in liquid films mobilized by continuous surfactant delivery. *Phys. Fluids* **15**, 3837–3845.

Frank, B. & Garoff, S. 1995 Origins of the complex motion of advancing surfactant solutions. *Langmuir* **11**, 87–93.

Gaver, D. P. & Grotberg, J. B. 1990 The dynamics of a localized surfactant on a thin film. *J. Fluid Mech.* **213**, 127–148.

Gaver, D. P. III, Halpern, D. & Jensen, O. E. 2005 Surfactant and airway liquid flows. In *Lung Surfactant and Disorder*. Lung Biology in Health and Disease, vol. 201 (ed. K. Nag). Taylor & Francis.

Grotberg, J. B. 1994 Pulmonary flow and transport phenomena. *Annu. Rev. Fluid Mech.* **26**, 529–571.

Grotberg, J. B. 2001 Respiratory fluid mechanics and transport processes. *Annu. Rev. Biomed. Engng* **3**, 421–457.

He, S. & Ketterson, J. B. 1995 Surfactant-driven spreading of a liquid on a vertical surface. *Phys. Fluids* **7**, 2640–2647.

Homsy, G. M. 1987 Viscous fingering in porous media. *Annu. Rev. Fluid Mech.* **19**, 271–311.

Jensen, O. E. 1994 Self-similar surfactant-driven flows. *Phys. Fluids* **6**, 1084–1094.

Jensen, O. E. 1998 The stress singularity in surfactant-driven thin-film flows. Part 2. Inertial effects. *J. Fluid Mech.* **372**, 301–322.

Jensen, O. E. & Grotberg, J. B. 1992 Insoluble surfactant spreading on a thin viscous film: shock evolution and film rupture. *J. Fluid Mech.* **240**, 259–288.

Jensen, O. E. & Halpern, D. 1998 The stress singularity in surfactant-driven thin-film flows. Part 1. Viscous effects. *J. Fluid Mech.* **372**, 273–300.

Joanny, J. F. 1989 Kinetics of spreading of a liquid supporting a surfactant monolayer: repulsive solid surfaces. *J. Colloid Interface Sci.* **128**, 407–415.

King, J. R. 2001 Thin-film flows and high-order degenerate parabolic equations. In *IUTAM Symposium on Free Surface Flows* (ed. A. C. King & Y. D. Shikmurzaev). Kluwer.

Krechetnikov, R. & Homsy, G. M. 2004 On a new surfactant-driven fingering phenomenon in a Hele-Shaw cell. *J. Fluid Mech.* **509**, 103–124.

Marmur, A. & Lelah, M. D. 1981 The spreading of aqueous surfactant solutions on glass. *Chem. Engng Commun.* **13**, 133–143.

Matar, O. K. & Troian, S. M. 1997 Linear stability analysis of an insoluble surfactant monolayer spreading on a thin liquid film. *Phys. Fluids* **9**, 3645–3657.

Matar, O. K. & Troian, S. M. 1998 Growth of non-modal transient structures during the spreading of surfactant coated films. *Phys. Fluids* **10**, 1234–1236.

Matar, O. K. & Troian, S. M. 1999*a* The development of transient fingering patterns during the spreading of surfactant coated films. *Phys. Fluids* **11**, 3232–3246.

Matar, O. K. & Troian, S. M. 1999*b* Spreading of a surfactant monolayer on a thin liquid film: Onset and evolution of digitated structures. *Chaos* **9**, 141–153.

Münch, A. 2003 Pinch-off transition in Marangoni-driven thin films. *Phys. Rev. Lett.* **91**, 016105.

Oron, A., Davis, S. H. & Bankoff, S. G. 1997 Long-scale evolution of thin liquid films. *Rev. Mod. Phys.* **69**, 931–980.

Ramé, E. 2001 The spreading of surfactant-laden liquids with surfactant transfer through the contact line. *J. Fluid Mech.* **440**, 205–234.

Starov, V. M., Kosvintsev, S. R. & Velarde, M. G. 2000 Spreading of surfactant solutions over hydrophobic substrates. *J. Colloid Interface Sci.* **227**, 185–190.

Stoebe, T., Lin, Z. X., Hill, R. M., Ward, M. D. & Davis, H. T. 1997 Enhanced spreading of aqueous films containing ethoxylated alcohol surfactants on solid substrates. *Langmuir* **13**, 7270–7275.

Troian, S. M., Herbolzheimer, E. & Safran, S. A. 1990 Model for the fingering instability of spreading surfactant drops. *Phys. Rev. Lett.* **65**, 333–336.

Troian, S. M., Wu, X. L. & Safran, S. A. 1989 Fingering instability in thin wetting films. *Phys. Rev. Lett.* **62**, 1496–1499.

Warner, M. R. E., Craster, R. V. & Matar, O. K. 2004*a* Fingering phenomena associated with insoluble surfactant spreading on thin liquid films. *J. Fluid Mech.* **510**, 169–200.

Warner, M. R. E., Craster, R. V. & Matar, O. K. 2004*b* Fingering phenomena created by a soluble surfactant deposition on a thin liquid film. *Phys. Fluids* **16**, 2933–2951.

Zhu, S., Miller, W. G., Scriven, L. E. & Davis, H. T. 1994 Superspreading of water-silicone surfactant on hydrophobic surfaces. *Colloids & Surfaces* A **90**, 63–78.